Proceedings of ASME Turbo Expo 2012
GT2012
June 11-15, 2012, Copenhagen, Denmark

GT2012-69742

LIFE PREDICTION FOR TURBOPROPULSION SYSTEMS UNDER DWELL FATIGUE CONDITIONS

Kwai S. Chan, ASME Fellow
Michael P. Enright
Jonathan P. Moody
Southwest Research Institute®
San Antonio, TX 78238, USA

Benjamin Hocking
Simeon H. K. Fitch
Elder Research Inc.
Charlottesville, VA 22903, USA

ABSTRACT

The objective of this investigation was to develop an innovative methodology for life and reliability prediction of hot-section components in advanced turbopropulsion systems. A set of three generic time-dependent crack growth models was implemented and integrated into the DARWIN® probabilistic life-prediction code. Using the enhanced risk analysis tool and material constants calibrated to IN 718 data, the effect of *time-dependent* crack growth on the risk of fracture in turboengine component was demonstrated for a generic rotor design and a realistic mission profile. The results of this investigation confirmed that time-dependent crack growth and cycle-dependent crack growth in IN 718 can be treated by a simple summation of the crack increments over a mission. For the temperatures considered, time-dependent crack growth in IN 718 can be considered as a K-controlled environmentally-induced degradation process. Software implementation of the generic time-dependent crack growth models in DARWIN provides a pathway for potential evaluation of the effects of multiple damage modes on the risk of component fracture at high service temperatures.

1 INTRODUCTION

Hot-section components in advanced turbopropulsion systems are often required to operate with long duration at high temperatures where time-dependent degradation mechanisms such as creep, oxidation, corrosion, and stress rupture may compete with time-independent fatigue crack growth as the component life-limiting mechanism. Thus, the effects of high heat dwell environment on the life and reliability of engine disks must be predicted accurately. These effects include the activation of synergistic time-dependent damage modes such as creep, stress corrosion, and stress rupture in the presence of cycle-dependent fatigue crack initiation and growth.

This investigation focused on addressing the effects of competing time-dependent damage modes including creep, stress corrosion, and stress rupture on long-term performance and reliability of engine disks made from Ni-based superalloys that could exhibit location-specific microstructures, microstructural variability or evolution of microstructures after thermal exposures at elevated temperatures for extended time periods. A novel time-dependent fracture algorithm was integrated with a commercial probabilistic life-prediction code, called DARWIN® [1], to complement a suite of existing capabilities including finite element analysis tools, fracture mechanics analysis tools, and reliability analysis tools. After implementation, this enhancement was utilized to demonstrate the potential use of such an analysis tool for estimating part life and reliability of a turbo engine subjected to aggressive mission profiles that contain long durations at high peak and dwell temperatures, which could lead to time-dependent damage modes such as creep, corrosion, and stress rupture.

One particular damage mode of interest was stress corrosion in the form of environmentally-enhanced crack growth, schematically shown in Fig. 1, caused by ingress of oxygen and material degradation by oxide formation along grain boundaries. It is envisioned that this methodology, upon further development, can be used to predict complex failure modes (such as creep, stress rupture, environmentally-assisted fracture, and stress corrosion) and make design improvements to counter these potential time-dependent, high-temperature damage modes.

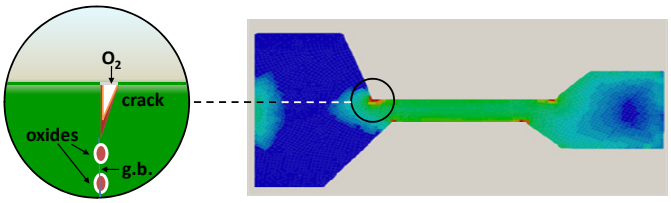

Fig. 1. The proposed methodology enables designers and analyst to perform life and reliability on hot-section components subject to aggressive mission profiles with high peak temperature and long dwell times that can lead to time-dependent damage modes such as creep, stress rupture, and stress corrosion. The DARWIN enhance-ments developed under this study will enable the analyst to compute reliability contours such as oxygen-assisted cracking along a grain boundary as shown schematically in this figure.

The approach to this investigation was based on the implementation of a set of three generic time-dependent crack growth models, their integration into DARWIN (a probabilistic life-prediction code [1]), and their demonstration in DARWIN via a problem constructed from representative data. This project was a joint effort of Mustard Seed Software, LLC (MSS), Charlottesville, Virginia, and Southwest Research Institute® (SwRI®), San Antonio, Texas, with significant support from Pratt & Whitney (P & W). Pratt & Whitney assisted by providing experimental data of IN 718 for formulating models and demonstrating the implementation, definition of the demonstration problem, and mission profile. The IN 718 data were generated by P & W as part of the Probabilistic Design for Rotor Integrity (PDRI) Program funded by the Federal Aviation Administration (FAA). This set of IN 718 data will be referred to as the PDRI data [2]. In addition, SwRI investigated and developed a framework for integrating the time-dependent crack growth module into MicroFaVa [3], a material microstructure analysis tool, that predicts macro scale material properties based on stochastic microstructural parameters.

This paper reports the work performed to develop a probabilistic framework for treating time-dependent crack growth in turbopropulsion components. The time-dependent crack growth models developed under this study are presented in Section 2. The cycle-dependent fatigue model is presented in Section 3, followed by the description of the combined time- and cycle-dependent models in Section 4. DARWIN demonstration of a probabilistic analysis of a turboengine component using the newly developed time-dependent crack growth analysis tool is described in detail in Section 5. Discussion of the effect of time-dependent crack growth, model implementations, and DARWIN demonstration results is presented in Section 6, followed by conclusions in Section 7.

2 DEVELOPMENT OF TIME-DEPENDENT CRACK GROWTH MODELS

The crack growth kinetics of time-dependent damage modes such as creep, stress corrosion, and stress rupture can generally be described in terms of the expression given by [4-8]

$$\frac{da}{dt} = B_1 K^{m_1} \tag{1}$$

where B_1 and m_1 are empirical constants, and K is the stress intensity factor. As illustrated in Fig. 2(a), this relationship is observed in the region $K_{th} < K < K_{IC}$, where K_{th} is the threshold stress intensity factor for the damage mode and K_{IC} is the critical stress intensity factor for unstable fracture when the process zone due to creep, corrosion, or oxidation-induced fracture is confined to and controlled by the elastic crack-tip stress field, i.e., the K-field. The material constants B_1 and m_1 depend on temperature, microstructure, alloy composition, and the operative damage mode.

Under transient creep conditions, the near-tip stress field is time-dependent and the crack growth kinetics are better described in terms of

$$\frac{da}{dt} = B_2 \left(\frac{K^2}{t} \right)^{m_2} \tag{2}$$

where B_2 and m_2 are empirical constants which depend on temperature, microstructure, alloy composition, and the operative damage mode [9]. This form of crack growth kinetics is typically associated with small-scale transient creep when the creep zone is still confined within the K-field. Its occurrence results in a range of frequency effects in the transition or mixed fracture zone located between the cycle-dependent crack growth regime at very high frequencies and the time-dependent crack growth regime at very low frequencies [4-7].

For environmentally-assisted crack growth, the crack growth kinetics may sometimes be controlled by transport of the embrittling species from the crack tip to the bulk by grain

boundary diffusion. Under this circumstance, the crack growth rate is a constant as given by

$$\frac{da}{dt} = B_3 \tag{3}$$

for $K_{th} < K < K_{IC}$, and B_3 is a material constant that depends on temperature, microstructure, alloy composition, and the embrittling species [10]. This crack growth process is illustrated schematically in Fig. 2(b). Eq. (3) can be considered as a special case of Eq. (1) with $m_1 = 0$.

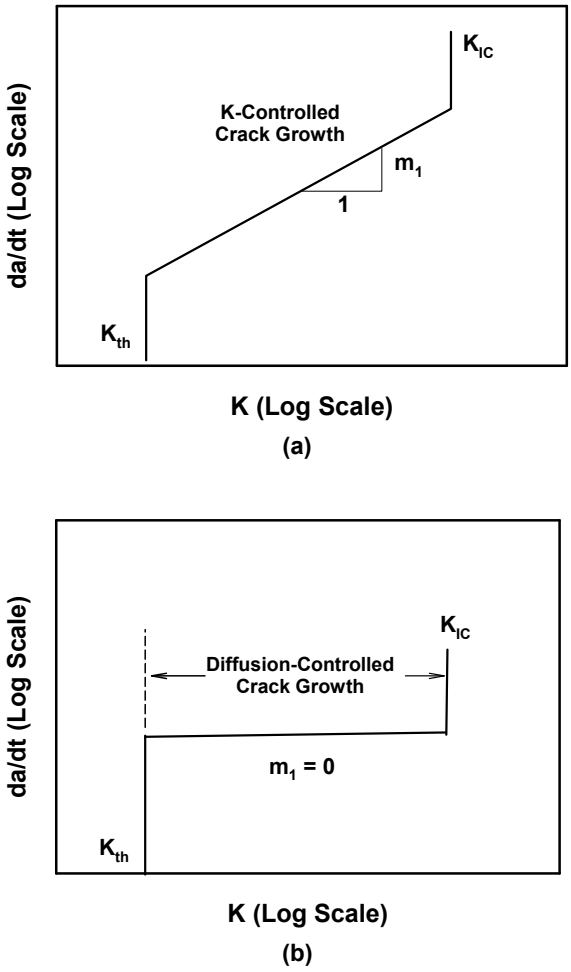

Fig. 2. Schematics of time-dependent crack growth curves of Ni-based superalloys at elevated temperatures: (a) K-controlled crack growth, and (b) diffusion-controlled crack growth.

IN 718 nickel alloy was selected for use in this investigation because its properties are well known and non-proprietary. Time-dependent crack growth data of IN 718 were obtained from P & W [2]. This set of experimental data included fatigue crack growth data (*da/dN*) subjected to dwell-time effects and creep crack growth data (*da/dt*) for two temperatures (1100°F and 1200°F) using surface-flawed and compact-tension specimens.

The IN 718 data [2] was utilized to evaluate Eqs. (1), (2), and (3) and the creep crack growth data was best described in terms of Eq. (1). In particular, a power law, Eq. (1), was fitted to these experimental results for surface-flawed specimens tested at 1100°F and 1200°F. The creep crack growth data of IN 718 at 1100°F and 1200°F, along with these power law fits, are presented in Fig. 3. For simplicity, the subscript 1 was dropped from B_1 and m_1 so that

$$\frac{da}{dt} = BK^m \tag{4}$$

where B and m are empirical constants obtained by fitting Eq. (4) to the experimental data in the power-law regime. Values of B and m for IN 718 are presented in Table 1. Both B and m appear to depend on the test temperature. A comparison of the *da/dt* data obtained using surface-flaw (SF) and compact-tension (CT) specimens, shown in Fig. 4, show the presence of a well-defined threshold in the CT specimen, but not in the SF specimens. In addition, fatigue crack growth tests with a 2-minute dwell showed the lower-bound threshold. Consequently, the lower bound threshold at 2-minute dwell tests was taken as the creep threshold for a particular temperature, as shown in Table 1. To expand the range of applicability, literature data for 1000°F [11-13] were also utilized and included in Table 1.

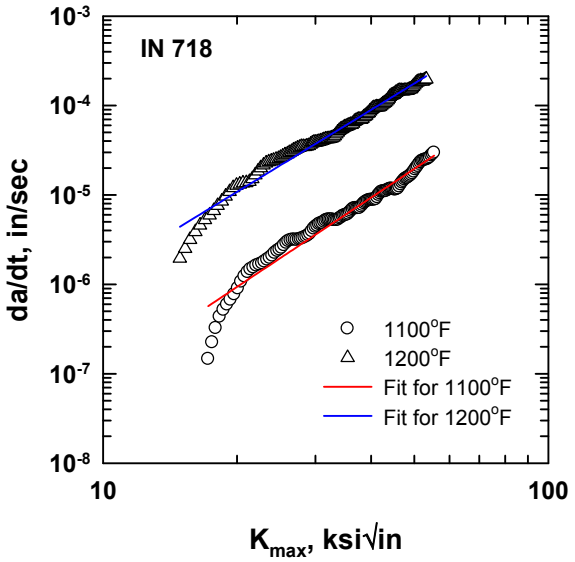

Fig. 3. Experimental data for crack growth at 1100°and 1200°F, with power law fits.

Table 1. Derived values of *B* and *m* for 1000°F, 1100°F and 1200°F.

Temperature, °F	*B*, in./sec/(ksi(in.)$^{1/2}$)^{m}	*m*	K_{th}, ksi(in.)$^{1/2}$
1000	2.30E-12	3.3178	13.5
1100	4.527E-11	3.3178	13.5
1200	1.190E-9	3.0436	13.0

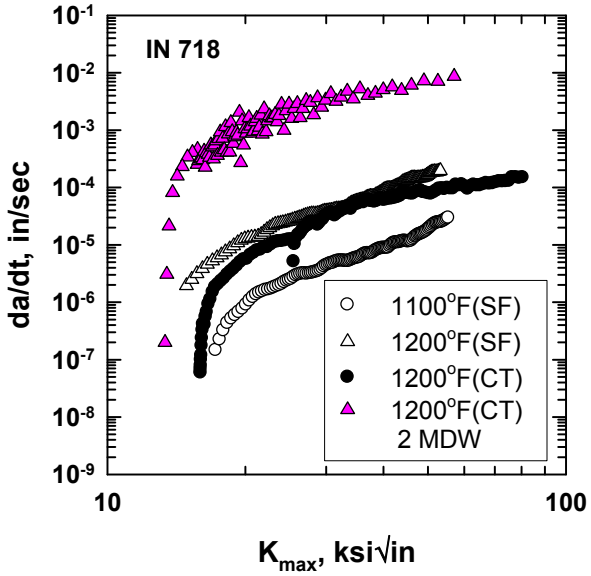

Fig. 4. A comparison of the da/dt data of IN 718 for SF and CT specimens without and with 2 minute dwell (2 MDW) from the PDRI dataset [2].

The temperature dependence of B was analyzed by expressing B in terms of an Arrhenius relation such that

$$\frac{da}{dt} = B_0 e^{-\frac{Q}{RT}} K^m \qquad (5)$$

B_0 is a constant, T is absolute temperature, R is the universal gas constant, and Q is the activation energy. Figure 5(a) shows a plot of B versus $1/T$. A regression analysis was used to obtain the slope and the intercept from which B_0 and Q were derived. The value of B_0 was determined to be 6.0E10 in/s/(ksi (in.)$^{1/2}$)^{m} and Q was 1.167E8 ft-lb/lb-mol°R.

For comparison with literature data, Fig. 5(b) presents a double-logarithmic plot of *da/dt* versus $1/T$ for IN 718 from the PDRI dataset [2], and two sets of IN 718 data from the literature (Browning [12] and Sadananda and Shaninian [13]). All three sets of *da/dt* data are for K = 25 ksi(in.)$^{1/2}$. Considerable scatter exists among the three sets of *da/dt* data. As a result, material constants were evaluated separately for individual alloys without mixing with these data.

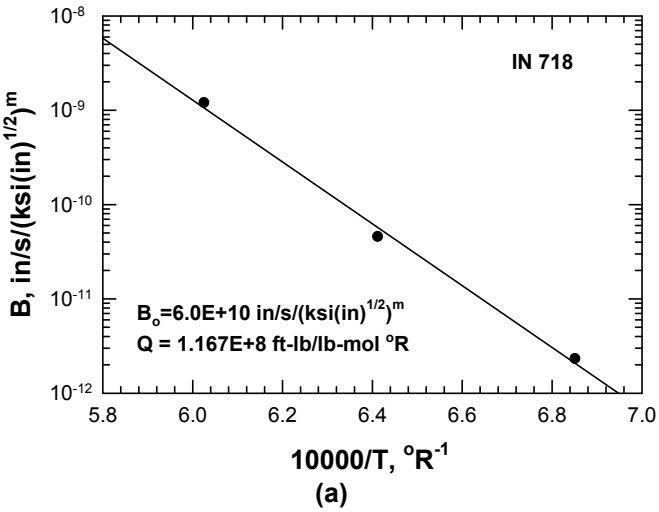

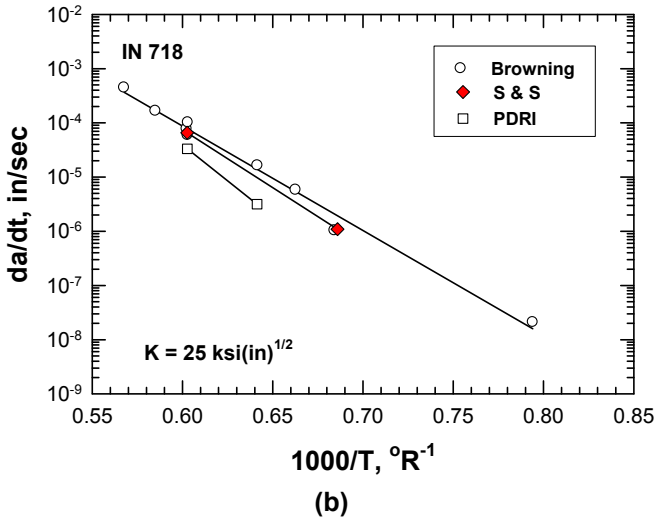

Fig. 5. (a) Log-log plot of *B* versus reciprocal absolute temperature for IN 718, and (b) log-linear plot of *da/dt* versus reciprocal absolute temperature for IN 718 from the PDRI dataset [2], Sadananda and Shaninian (S&S) [13], and Browning [12].

The B_0 parameter can be related to the degradation zone [14], leading to

$$B_0 = \frac{\alpha_p}{t_0 K_0^m} \tag{6}$$

where α_p is the penetration depth coefficient, t_0 is the reference time, and K_0 is the reference stress intensity factor. Since B_0 is a constant (B_0 = 6 E+10 in./s), α_p = 1.0 E+9 in after K_0 was taken to be 0.91 ksi√in. and t_0 = 60s. It is noted that the material constants were determined initially in the SI units. K_0 and t_0 were chosen to be 1 MPa√m and 60s for convenience, which converted to 0.91 ksi√in. and 60s in the US customary units.

The IN 718 data from the PDRI Program [2] was combined with additional data of IN 718 from the literature to determine the extent of time-dependent crack growth in Fig. 6, which depicts *da/dN* as a function of frequency at a constant ΔK of 25 ksi(in.)$^{1/2}$. Figure 6 shows that the cyclic crack growth rate, *da/dN*, in air environment is independent of the frequency at temperatures below 750°F. In contrast, time-dependent crack growth is apparent in air environments for temperatures at or above 1000°F. One study showed that *da/dN* in vacuum at 1200°F is independent of frequency, suggesting that time-dependent crack growth in IN 718 in air may be an environmentally-induced degradation process such as oxidation or corrosion [14].

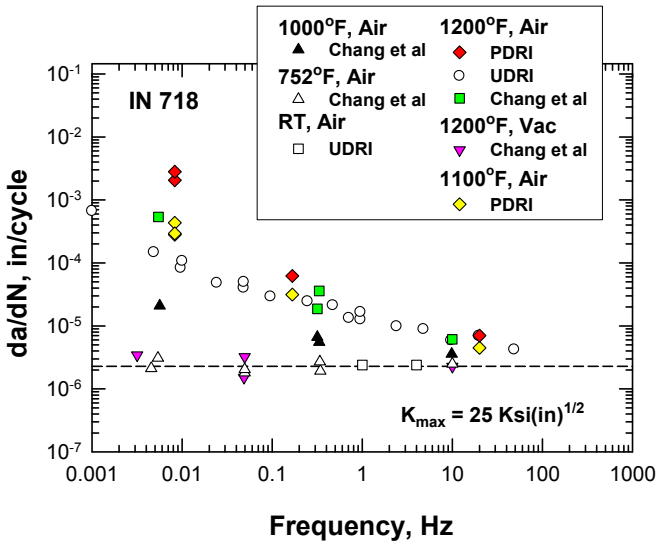

Fig. 6. Fatigue crack growth rate of IN 718 at K = 25 ksi(in)$^{1/2}$ as a function of frequency at various temperatures. Time-dependent fatigue crack growth is observed only in air at temperatures at or above 1000°F. Cycle-dependent fatigue crack growth is observed in IN 718 at temperatures at or below 750°F and at 1200°F in vacuum. IN 718 data are from the PDRI dataset [2], UDRI [6], and Chang et al. [11].

3 DEVELOPMENT OF CYCLE-DEPENDENT CRACK GROWTH MODELS

The fatigue crack growth rate, *da/dN,* was represented in terms of the Paris power-law [15], as given by

$$\frac{da}{dN} = A\Delta K^n \quad \text{for } \Delta K > \Delta K_{th} \tag{7}$$

where ΔK is the stress intensity range, ΔK_{th} is the large-crack crack growth threshold, and A and n are material constants. A summary of the material constants for IN 718 is presented in Table 2. The material constants for 1100°F and 1200°F were derived from the PDRI data [2], while those for ambient temperature are from the literature [16].

4 COMBINED TIME- AND CYCLE-DEPENDENT CRACK GROWTH MODEL

Cycle-dependent fatigue crack growth and time-dependent crack growth are generally treated as two independent processes whose crack growth increment, da, over a mission can be summed according to the expression given by [8]

$$(da)_{mission} = \left(\frac{da}{dN}\right)_{cyclic} dN + \left(\frac{da}{dt}\right) dt \tag{8}$$

where the first term on the right-hand-side of Eq. (8) treats cycle-dependent crack growth while the second term treats time-dependent crack growth for an arbitrary loading history

Table 2. Derived values of *A* and *n* for IN 718 at 1000°F, 1100°F and 1200°F

Temperature, °F	*A*, in./cycle/(ksi(in.)$^{1/2}$)^m	*n*	ΔK_{th}, ksi(in.)$^{1/2}$
75	1.56E-11	3.66	7.5
1100	4.41E-10	3.18	7.5
1200	7.27E-10	3.23	7.0

within a mission. This approach was implemented in DARWIN and the same approach was utilized to experimental data from laboratory test specimens and correlation of model calculation and experimental data.

For fatigue crack growth test data generated under a constant frequency with dwell, Eq. (8) can be expressed as

$$\left(\frac{da}{dN}\right)_{dwell} = \left(\frac{da}{dN}\right)_{cyclic} + \left[t_{dwell} + 1/f\right]\left(\frac{da}{dt}\right) \qquad (9)$$

where t_{dwell} is the dwell time and f is the frequency. Eq. (9) was applied to compute the fatigue crack growth response of IN 718 with dwell at 1100°F and 1200°F using the fatigue crack growth model, Eq. (7), and the time-dependent crack growth model, Eq. (5), with the experimental frequency and dwell time. Figures 7(a) and (b) present comparisons of the model predictions and experimental results for 1000°F and 1200°F, respectively. In Fig. 7(a), *da/dN* at 20Hz, *da/dt,* and *da/dN* with a 2-minute dwell (2 MDW) at the load are compared for 1100°F. It should be noted that the *da/dN* curve at 20Hz and the *da/dt* curve exhibit comparable crack growth rates for the unit chosen or at a one-second dwell time at a slow frequency for *da/dt* (see Eq. (9)). In contrast, the *da/dN* with 2-minute dwell shows considerably higher crack growth rates at similar K levels because substantial crack extension occurs during the dwell period. Similar results and comparisons are shown in Fig. 7(b) for 1200°F. Again, the *da/dN* response for the 2-minute dwell is significantly higher than those of *da/dN* at 20Hz and *da/dt* because of the contribution of time-dependent crack growth during the dwell period.

An evaluation of Eq. (9) was performed by computing the fatigue crack growth rate at K = 25 ksi(in.)$^{1/2}$ as a function of frequency for 1100°F and 1200°F. A comparison of the predicted *da/dN* versus the PDRI data [2] is presented in Fig. 8. In this plot, *da/dN* data with dwell are included by approximating the effective frequency during dwell as 1 over the dwell time. The interaction of cycle-dependent and time-dependent crack growth at elevated temperatures and low frequency are evident in Fig. 8.

A more detailed evaluation of Eq. (9) was performed by computing the fatigue crack growth rate at K = 25 ksi(in.)$^{1/2}$ as a function of frequency for temperatures from 75°F and 1200°F. Comparison of the predicted *da/dN* versus the PDRI data [2] and additional IN 718 data from the literature [6, 11] is presented in Fig. 9. The cyclic *da/dN* term dominates at low temperatures (< 750°F). In contrast, the time-dependent crack growth term starts to become important at temperatures at or above 1000°F. For IN 718, Eq. (9) appears to be adequate for treating cycle-dependent and time-dependent crack growth over a wide range of frequencies for temperatures ranging from 75°F to 1200°F.

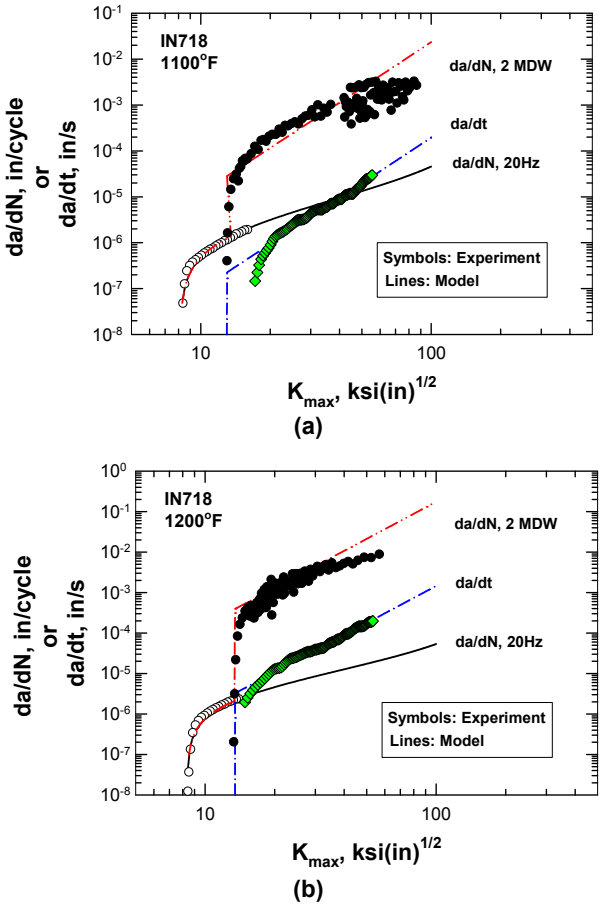

Fig. 7. Comparisons of computed and measured fatigue crack growth response of IN 718 with and without a 2 min. dwell (2 MDW): (1) 1100°F, and (b) 1200°F. Experimental data are from the PDRI Program [2].

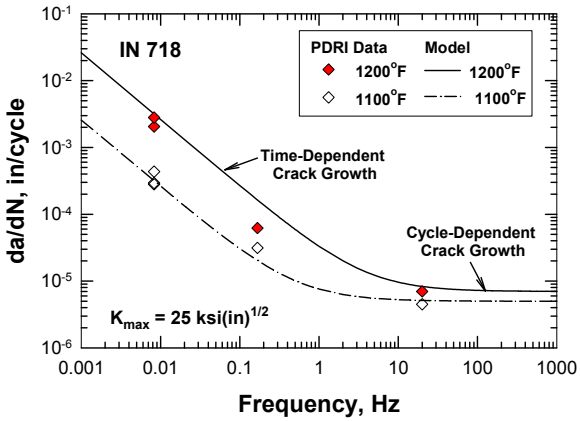

Fig. 8. Comparison of computed and measured fatigue crack growth response of IN 718 at K = 25 ksi(in.)$^{1/2}$ as a function of frequency for 1100°F and 1200°F. Experimental data are from the PDRI Program [2].

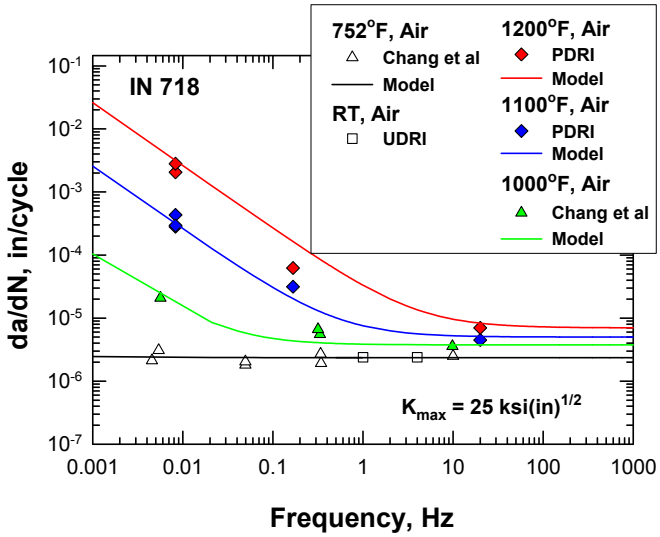

Fig. 9. Comparison of computed and measured fatigue crack growth response of IN 718 at K = 25 ksi(in)$^{1/2}$ as a function of frequency at various temperatures ranging from 75°F to 1200°F. Experimental data are from the PDRI Program [2], UDRI [6], and Chang et al. [11]

5 DARWIN Demonstration Problem

For the purposes of verifying the effects of high-temperature time-based fatigue, a realistic reliability analysis demonstration problem was needed. It consists of the following major components:

- The material properties of a well-known alloy formulation defining the constants used in the time-dependent crack growth equations implemented in DARWIN.
- Generic, non-proprietary axisymmetric rotor geometry definition of realistic complexity and size.
- Stress and temperature load step definitions for a selected gas turbine rotor disk geometry with associated mission profile and load step durations.

IN 718 was selected as the model alloy for the DARWIN demonstration. The finite-element (FE) model of a rotor design selected for this demonstration problem is shown in Fig. 10. A mission profile consisting of stress and temperature as a function of time and load step durations was provided by P & W. This mission profile, which cannot be presented here because of proprietary reasons, contained pertinent temperature, stress, and time histories that were necessary to test the time-dependent crack growth model presented in this paper. A surface anomaly in the form of a half-penny-shaped crack was assumed to be present near a bore, and the surface anomaly distribution is shown in Fig. 11. The median of the initial crack depth was 0.012 in. Two probabilistic crack growth analyses were performed: one with and one without concurrent time-dependent crack growth during cycle-dependent fatigue crack growth. Cycle counting was performed using a rain-flow method.

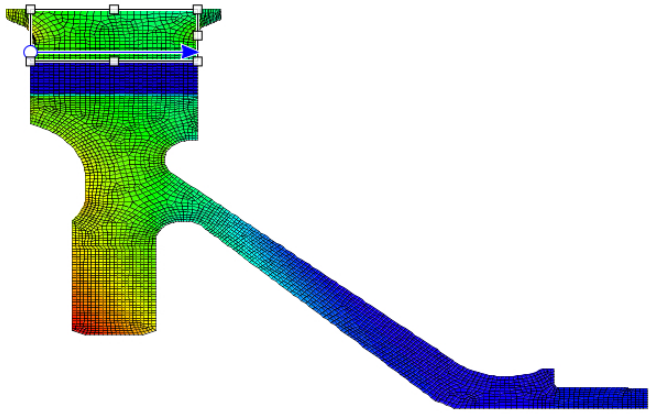

Fig.10. Finite-element model of a gas turbine rotor design selected for the time-dependent crack growth demonstration problem using DARWIN.

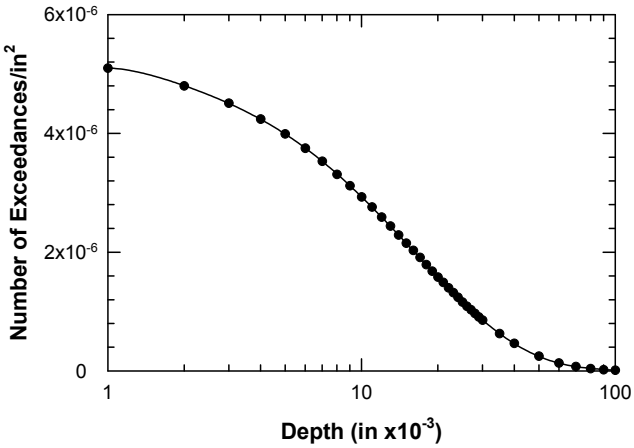

Fig. 11. Surface anomaly distribution utilized in the DARWIN demonstration problem.

Some of the results of the demonstration problem are highlighted in Figs. 12 to 14. Figure 12 plots the value of K_{max} as a function of flight cycles, while Fig. 13 presents the corresponding cracked area as a function of flight cycles. In both figures, the actual values of K_{max} and cracked area were intentionally left out in order to protect sensitive data. Figure 14 presents results of the conditional probability of fracture due to fatigue crack growth with and without concurrent time-dependent crack growth. As expected, the fatigue life was reduced and the risk of fracture was increased by time-dependent crack growth. Thus, the time-dependent crack growth framework implemented in DARWIN appeared to work properly and successfully in this demonstration problem.

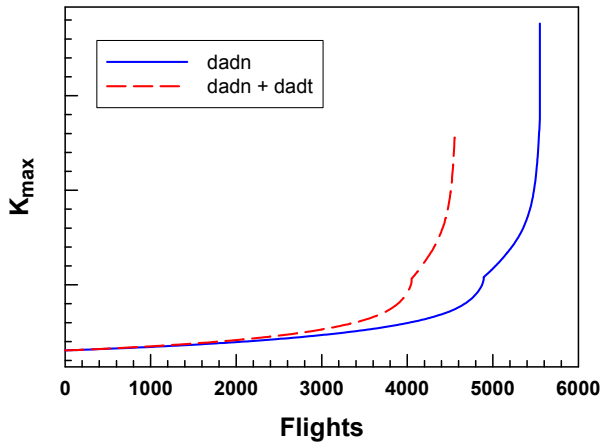

Fig. 12. DARWIN results of maximum stress intensity, K_{max}, as a function of flight cycle for the demonstration problem.

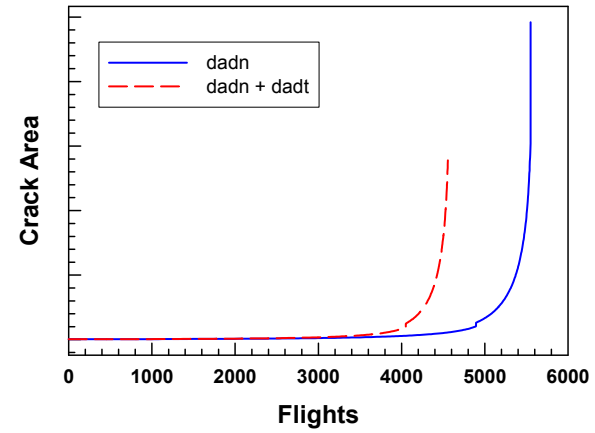

Fig. 13. DARWIN results of cracked area as a function of flight cycle for the rotor design used in the demonstration problem.

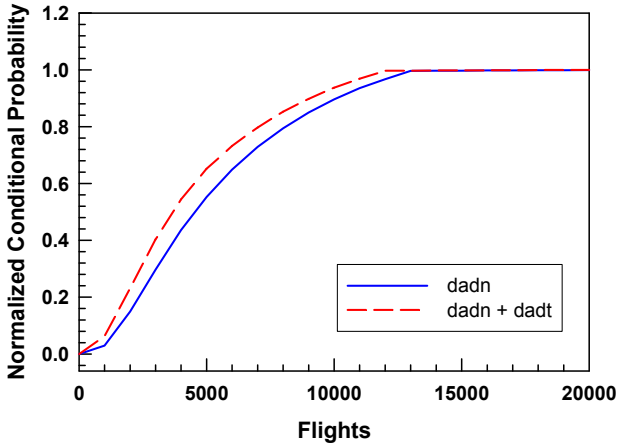

Fig.14. Computed conditional probability of fracture as a function of flight cycle for the rotor design used in the demonstration problem.

6 DISCUSSION

The results of this investigation suggest that time-dependent crack growth and cycle-dependent crack growth in IN 718 can be treated by a simple summation of the crack increments over a mission, as described in Eq. (8) and validated by laboratory test data shown in Figs. 7-9. Such an approach is applicable over a wide range of frequencies and temperatures, as shown in Figs. 7-9. From Fig. 7, it is evident that the dwell time at peak temperature can significantly impact the risk of fracture for mission profiles that contain long-term dwell at high temperatures. The time-dependent crack growth framework implemented in DARWIN can be used to predict the increase in disk risk due to oxidation, stress corrosion, and environmentally induced crack growth.

For the temperatures considered, time-dependent crack growth in IN 718 can be considered as a K-controlled environmentally-induced degradation process, as the *da/dN* and *da/dt* behaviors can be described in terms of ΔK and K_{max} as the crack-driving force, respectively. For both processes, a power law of the Paris type with a positive power-law exponent is observed. Thus, the kinetics of time-dependent crack growth is not controlled or limited by diffusion of an embrittling specie such as oxygen, and Eq. (3) is not applicable for IN 718. Figure 6 also indicates that time-dependent crack growth in IN 718 ceases to occur at 1200°F in vacuum. This observation suggests that creep is not responsible for the time-dependent crack growth observed in air. Hence, Eq. (2) can also be ruled out for IN 718. Taking all experimental evidence into consideration, time-dependent crack growth in IN 718 appears to originate from oxidation or stress corrosion.

The initial depth of the surface anomaly used in the demonstration problem was 12 mil. Such a large anomaly size was needed in order to overcome the relatively high threshold values (K_{th} > 13 ksi(in.)$^{1/2}$) for the onset of time-dependent crack growth at temperatures greater than 1000°F. The corresponding ΔK_{th} is about 7.5 ksi(in.)$^{1/2}$ at these temperatures. Thus, time-dependent crack growth in IN 718 is prevalent at high K levels, high temperatures, and long dwell times. All of these conditions were met by the mission profile utilized in the demonstration problem.

In the demonstration problem, only the anomaly size was treated as a random variable. Variability in *da/dt*, which is evident in Fig. 6, and K_{th}, which is evident in Fig. 4, has not been considered. Although the time-dependent crack growth framework developed in this study includes three types of generic crack growth behavior, only the K-controlled crack growth relation, Eq. (1), was utilized and evaluated because IN 718 does not exhibit crack growth behaviors described by Eqs. (2) and (3) in the temperature range considered in the demonstration problem. In future work, material variability, multiple damage modes, and spectrum loading will be investigated to assess the corresponding risk to disk failure.

7 CONCLUSIONS

A set of three generic time-dependent crack growth models has been implemented and integrated into the DARWIN probabilistic life-prediction code. Using the enhanced risk analysis tool, the effect of time-dependent crack growth on the risk of fracture in turboengine components was demonstrated for a rotor design based on IN 718 and a mission profile provided by Pratt & Whitney. The conclusions reached in this study are as follows:

1. Time-dependent crack growth in an IN 718 rotor was successfully demonstrated using a realistic anomaly defect distribution and mission profile.
2. Time-dependent crack growth in IN 718 is K-controlled and originates from oxidation or stress corrosion.
3. Summation of cycle-dependent and time-dependent crack growth rates integrated over the mission profile is applicable to IN 718 and the mission profile considered.
4. Time-dependent crack growth results in a decrease in crack growth life and an increase in risk of fracture in the rotor design considered in the demonstration problem.
5. The *da/dN* of IN 718 is higher in dwell fatigue compared to *da/dN* at high frequency or *da/dt* at identical K levels because the crack extension during dwell is the product of *da/dt* and the dwell time. A larger dwell time thus leads to a higher *da/dN* during dwell fatigue.
6. Software implementation of the generic time-dependent crack growth models in DARWIN provides a pathway for potential evaluation of the effects of one or more damage modes on the risk of component fracture at high service temperatures.

ACKNOWLEDGEMENTS

This work was supported by NAVAIR under contract No. N68335-11-C-0171 and monitored by Mr. Randy A. Pickering. The authors are thankful for the support of Pratt & Whitney in providing the IN 718 data and the mission profile used in this study. The assistance by Ms. Loretta Mesa, SwRI, in the preparation of the manuscript is acknowledged.

REFERENCES

1. DARWIN® User's Guide. Southwest Research Institute, 2011, San Antonio, TX.
2. *Probabilistic Design for Rotor Integrity (PDRI) Interim Report 9*, Southwest Research Institute, March 4, 2010. The tests were performed by Pratt & Whitney and funded under FAA Grant 05-G-005.
3. K.S. Chan and M.P. Enright, "A Probabilistic Micro-mechanical Code for Predicting Fatigue Life Variability: Model Development and Application," *ASME Journal of Engineering for Gas Turbines and Power*, 2006, Vol. 128, pp. 889-895.
4. T. Nicolas, T. Weerasooriya, and N.E. Ashbaugh, "A Model for Creep/Fatigue Interactions in Alloy 718," *Fracture Mechanics: Sixteenth Symposium, ASTM STP 868*, M.H. Kanninen and A.T. Hopper, Eds., ASTM, Philadelphia, PA, 1985, pp. 167-180.
5. T. Nicolas and T. Weerasooriya, "Hold-Time Effects in Elevated Temperature Fatigue Crack Propagation," *Fracture Mechanics: Seventeenth Symposium, ASTM STP 905*, J.H. Underwood et al., Eds., ASTM, Philadelphia, PA, 1986, pp. 155-168.
6. T. Weerasooriya, "Effect of Frequency on Fatigue Crack Growth Rate of Inconel 718 at High Temperature," AFWAL-TR-4038, Univ. of Dayton, Dayton, OH, June 1987.
7. D.A. Woodford, "Gas Phase Embrittlement and Time Dependent Cracking of Nickel-Based Superalloys," *Energy Materials*, Vol. 1, No. 1, pp. 59-79.
8. R.H. Van Stone and D.C. Slavik, "Prediction of Time-Dependent Crack Growth with Retardation Effects in Nickel Base Alloys," *Fatigue and Fracture Mechanics: 31st Volume, ASTM STP 1389*, G.R. Halford and J. P. Gallagher, Eds., ASTM, West Conshohocken, PA, 2000, pp. 405-426.
9. A. Saxena, "Creep Crack Growth under Non-Steady-State Conditions," *Fracture Mechanics: Seventeenth Symposium, ASTM STP 905*, J.H. Underwood et al., Eds., ASTM, Philadelphia, PA, 1986, pp. 185-201.
10. B.F. Brown, Ed., *Stress Corrosion Cracking in High-Strength Steels and in Titanium and Aluminum Alloys,* Naval Research Laboratory, Washington, DC, 1972.
11. K.-M. Chang, M.F. Henry, and M.G. Benz, "Metallurgical Control of Fatigue Crack Propagation in Superalloys," *JOM,* Dec. 1990, pp. 29-35.
12. P.F. Browning, "Time-Dependent Crack Tip Phenomena in Gas Turbine Disk Alloy," PhD Rensselaer Polytechnic Institute, NY, 1988; cited by D.A. Woodford, *Energy Materials*, 2006, Vol. 1, No. 1, pp. 59-79.
13. K. Sadananda and P. Shaninian, in *Creep-Fatigue Environment Interactions*, R.M. Pelloux and N.S. Stoloff, Eds., TMS-AIME, 1979, pp. 86-111.
14. J.J. McGowan and H.W. Liu, "A Kinetic Model for High Temperature Fatigue Crack Growth," Fatigue-Environment and Temperature Effects*, J.B. John and V. Weiss*, Eds., Plenum Press, NY, 1983, pp. 377-390.
15. P.C. Paris and F. Erdogan, "A Critical Analysis of Crack Propagation Law," *Transactions of the ASME, Journal of Basic Engineering*, Series D, Vol. 85, No. 3, 1963.
16. L.A. James and W.J. Mills, "Effect of Heat-Treatment and Heat-to-Heat Variations in the Fatigue-Crack Growth Response of Alloy 718," *Engineering Fracture Mechanics,* Vol. 22, 1985, pp. 797-817.